Spring 5-31-2012

Experimental evaluation of near infrared light penetration into neural tissue

Ujwal Anil Parikh

New Jersey Institute of Technology

Copyright Warning & Restrictions

The copyright law of the United States (Title 17, United States Code) governs the making of photocopies or other reproductions of copyrighted material.

Under certain conditions specified in the law, libraries and archives are authorized to furnish a photocopy or other reproduction. One of these specified conditions is that the photocopy or reproduction is not to be "used for any purpose other than private study, scholarship, or research." If a, user makes a request for, or later uses, a photocopy or reproduction for purposes in excess of "fair use" that user may be liable for copyright infringement,

This institution reserves the right to refuse to accept a copying order if, in its judgment, fulfillment of the order would involve violation of copyright law.

Please Note: The author retains the copyright while the New Jersey Institute of Technology reserves the right to distribute this thesis or dissertation

Printing note: If you do not wish to print this page, then select "Pages from: first page # to: last page #" on the print dialog screen

ABSTRACT

EXPERIMENTAL EVALUATION OF NEAR INFRARED LIGHT PENETRATION INTO NEURAL TISSUE

by
Ujwal Anil Parikh

Near infrared (NIR) lasers find applications in medicine both for diagnostic and treatment purposes. Penetration depth into the tissue is a critical parameter to be considered in these NIR laser applications. Published data on the optical properties of rodent neural tissue are rare, despite the frequent use of rats as animal models. The aim of this study was to directly measure the light intensity profile inside the rat brain gray matter that is illuminated by an NIR laser beam. The local light intensities were sampled using an optical fiber inserted into the brain. The intensity profile in the axial direction to the laser beam had an initial fast decreasing phase followed by a less steeper slope by distance. In general, the light penetrated several times farther in the direction of the beam than its spread in the radial direction.

EXPERIMENTAL EVALUATION OF NEAR INFRARED LIGHT PENETRATION INTO NEURAL TISSUE

by
Ujwal Anil Parikh

A Thesis
Submitted to the Faculty of
New Jersey Institute of Technology
in Partial Fulfillment of the Requirements for the Degree of
Master of Science in Biomedical Engineering

Department of Biomedical Engineering

May 2012

APPROVAL PAGE

EXPERIMENTAL EVALUATION OF NEAR INFRARED LIGHT PENETRATION INTO NEURAL TISSUE

Ujwal Anil Parikh

Dr. Mesut Sahin, Thesis Advisor
Associate Professor of Biomedical Engineering, NJIT Date

Dr. Sergei Adamovich
Associate Professor of Biomedical Engineering, NJIT Date

Dr. Bryan Pfister
Associate Professor of Biomedical Engineering, NJIT Date

BIOGRAPHICAL SKETCH

Author: Ujwal Anil Parikh

Degree: Master of Science

Date: January 2013

Undergraduate and Graduate Education:

- Master of Science in Biomedical Engineering,
  New Jersey Institute of Technology, Newark, NJ, 2013

- Bachelor of Engineering in Biomedical Engineering,
  University of Mumbai, Mumbai, India, 2008

Major: Biomedical Engineering

Publications:

Ammar Abdo, Ujwal Parikh, Mesut Sahin, "NIR Light Penetration Profile into the Rat Brain Gray Matter", 34th Annual International IEEE EMBS Conference (EMBS'12), Boston, MA, USA, August 2012.

ACKNOWLEDGEMENTS

I would like to thank Dr. Mesut Sahin for his supervision, guidance and advice. Without his support, this study would have been much harder and taken longer time. I would also like to acknowledge Dr. Sergei Adamovich and Dr. Bryan J. Pfister for actively participating in the committee. I am grateful to Ammar Abdo for his assistance in the experiments. Special thanks to John Hoinowski for helping with the mechanical parts needed in this study.

TABLE OF CONTENTS

TABLE OF CONTENTS
(Continued)

LIST OF TABLES

LIST OF FIGURES

LIST OF FIGURES
(Continued)

CHAPTER 1

INTRODUCTION

Optical methods using near infrared (NIR) lasers is an emerging technology offering numerous therapeutic and diagnostic applications. NIR light has been widely investigated for a variety of biomedical applications ranging from spectroscopic imaging [1] to treatment of brain tumors [2]. NIR wavelengths approximately between 700 to 900nm offer maximum penetration in the gray and white matters of the nervous system due to minimal absorption and scattering [3]. They offer the advantage of being non-ionizing and therefore, repeated exposures can be applied to the tissue.

In these applications, the penetration depth is a critical factor that needs to be determined. There are several reports on the optical properties of neural tissues [2, 4, 5]. However, data on the penetration depth in the neural tissue is rare and the results vary substantially [3, 6]. Also, studies on the rat nervous system are very limited. Rat has frequently been used as an animal model in testing of these laser applications [7]. The aim of this study was to determine the light intensity of NIR light at different depths inside the rat brain gray matter.

1.1 Objective

The objective of this study is to investigate the penetration profile of the NIR light in a 2D vertical plane into the rat brain cortex. To achieve the desired goals, this study was performed on two Sprague- Dawley rats using a laser operating at 830nm. A fiber optic was inserted into the brain to measure the light intensity at different depths of the brain

gray matter. As the current produced by the photodiode depends on the intensity of transmitted light reaching the diode; by measuring the current values at different depths we could study the amount of light intensity available at the given depth of the brain. The current values are then used to produce a graph of light intensity vs. depth. The shape of the curve is compared with the published data to validate the result.

1.2 Background Information

1.2.1 Penetration Depth of NIR Light in the *in vitro* Rat Brain Slices

In a previous study, the penetration depth into the gray matter of the rat brain was analyzed using an *in vitro* preparation [8]. The brain was explanted directly after sacrificing the animal and placed in sucrose cutting media. Horizontal brain slices were cut at thicknesses of 300, 400, 500, 600, 800, 1000, 1200, and 1500μm. *In vitro* measurements were conducted for each thickness using a photodiode and a laser source. The brain slices were laid down on the bottom surface of a petri dish, aligning an area of gray matter over and in direct contact with the photodiode and the laser was centered above at a distance of 15cm. The light intensity values were obtained for various thicknesses of the gray matter samples. Monte Carlo simulations were used to simulate the light intensity curve for each tissue thickness. The scattering coefficient was measured by manually adjusting the simulated light intensity to curve fit the experimentally calculated light intensity.

The mean light intensity of the gray matter was 65.03±0.02%, 44.87±0.02%, 32.16±0.02%, 22.68±0.03%, 14.14±0.01%, 7.78±0.005%, 5.38±0.005%, and 3.02±0.004% at thicknesses of 300, 400, 500, 600, 800, 1000, 1200, and 1500μm

respectively. The experimental values decline close to an exponential curve, whereas the simulations follow a curve similar to a low-pass filter deviating from the experimental values particularly at smaller thicknesses. The scattering coefficient was calculated as 108cm^{-1} by curve fitting the measured light intensity values with Monte Carlo simulations.

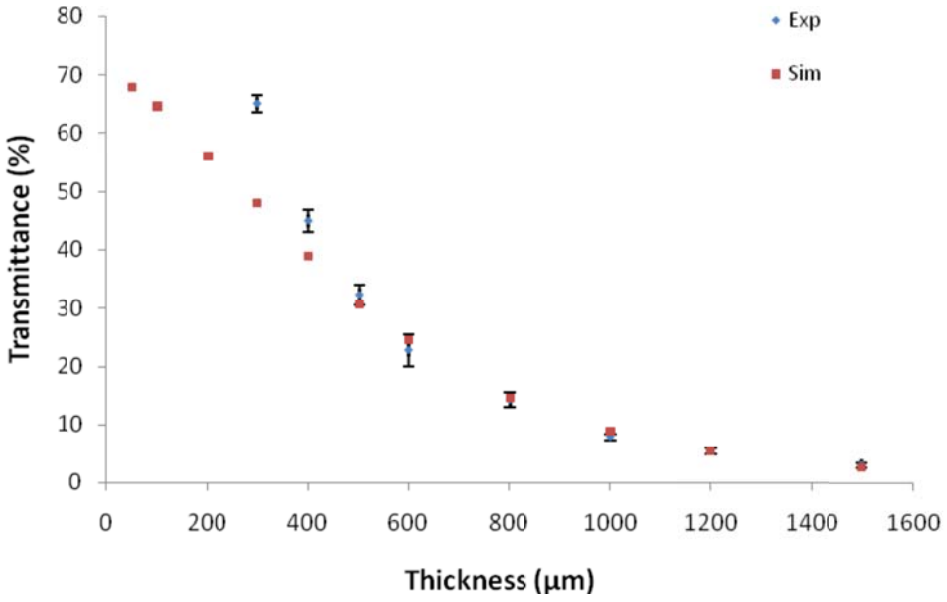

Figure 1.1 The experimental and simulated light intensity as a function of slab thickness. Experimental values for each thickness are an average of eight brain samples. The simulated values are fitted to the experimental ones by adjusting the scattering coefficient. The two plots differ significantly at the smallest thicknesses used, e.g., 300 and 400µm [8].

The light intensity curve for the simulated value and the experimentally found value is shown in Figure 1.1. These results were consistent with the findings of other published data. The values reported indicated that the light intensity was reduced to 3% of its original value within 1.5mm from the tissue surface (Figure 1.1). A smaller scattering coefficient yields larger penetration depths in general. Comparing the values of the scattering coefficient for the gray matter of rats with that of humans suggested a penetration depth that is a few times larger in the rat than humans. As shown in Figure

1.1, the Monte Carlo simulation matched the experimental values of light intensity very closely above 400μm. Monte Carlo simulations may also present unstable results at small thicknesses. If the data points at 300 and 400μm were excluded, the average error for the curve fit reduced to 6.3% (from 9.9%). The results suggested that the light intensity plot did not follow an exponential decay as predicted by the Beer's Law, that the plot had a plateau at small slab thicknesses (see Tsim in Figure 1.1).

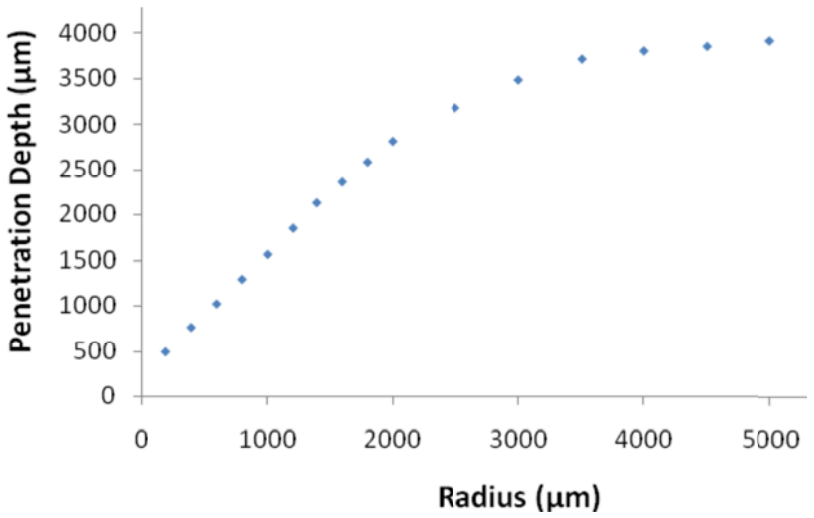

Figure 1.2 Penetration depths as a function of beam radius while the total beam energy is fixed. The penetration depth is defined as the depth where the incident light is reduced down to 37% of the original value. The beam radius is defined as two times the standard deviation of the Gaussian beam profile. The plot reaches a maximum for radius values larger than 3750μm [8].

Beam radius is an important factor in the NIR laser applications. As shown in Figure 1.2, light penetrated deeper into the tissue as the beam radius increased above a certain value. Thus, larger beam sizes are preferable in order to minimize the total NIR exposure while maintaining a certain photon density at the deep targets. Sample preparation techniques played a vital role in measurements of tissue optical properties. Shock and slow freezing temperatures can alter optical properties of biological tissues. The freezing procedure can change the optical properties by damaging the tissue due to

mechanical forces generated by ice crystals. Thus, in this study the explanted brain samples were not frozen or compressed. Samples were placed in cold sucrose solution (0^{o}C), without any direct contact to ice, to cut them into intact slices.

To summarize, the study reported these results:

i. The light intensity curve did not follow like a second order filter as predicted by simulations.
ii. The scattering co-efficient of the rat brain gray matter was found to be 108cm^{-1} which was within range of the published data.
iii. The penetration depth was a function of beam radius and increased with the beam radius up to a certain value.
iv. By taking adequate precaution in tissue slice preparation, robust measurements can be achieved.

1.2.2 Use of Near Infrared and Visible Spectroscopy to Determine Optical Properties of the Rat Neural Tissue

The goal of another study was to determine changes in the light scattering and hemoglobin oxygen saturation in three cases: (i) a normal spinal cord, (ii) demyelinated sciatic nerve, and (iii) spinal cord under neuronal activity induced by peripheral electrical stimulation [9]. However, the scope of this study was restricted only to the measurement of light scattering in a healthy spinal cord. Fourteen adult male Sprague-Dawley rats (250-350g) were used for this study. Laminectomy was performed to expose the thoracic and lumbar regions of the spinal cord. After the surgery the rats were immobilized on a stereotaxic frame and the optical reflectance measurements were made using a light

source, a bifurcated fiber optic and a spectrometer. The incident optical signal was generated by a tungsten-halogen light source and delivered to the tissue through the probe. The optical reflectance signals from the tissue were collected by the same probe and converted to electrical signals by a portable, real-time display spectrometer in the wavelength region of 450nm to 1000nm. The bifurcated probe contained two fibers, one acting as the source and the other as a detector, each with a diameter of 100 microns. The optic fiber probe was placed near lumbar level 5 (LL5) region of the rat spinal cord at a height of 575 microns above the exposed spinal cord surface, while the surface was covered with mineral oil (Figure 1.3).

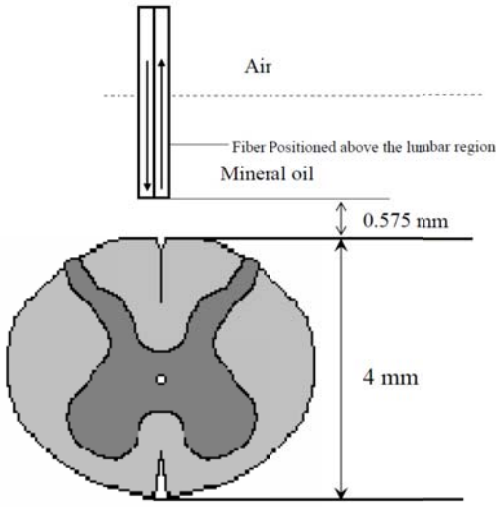

Figure 1.3 Cross section view of the lumbar region of the spinal cord. The darker region is gray matter surrounded by the lighter region of white matter, and the diameter of this section of the spinal cord is around 4mm [9].

The optical reflectance were recorded from three regions of the exposed rat spinal cord, i.e., left lumbar, right lumbar, and the blood vessel running near the center of the cord. From each region, the data were recorded at 1mm intervals rostrally starting from LL5. The raw reflectance data was plotted against the wavelengths 700nm – 850nm without calibration to get a graph called as the spectral slope. Further processing was

done to quantify the reduced scattering coefficient, μ_s' using a calibrated spectrum taken from the standard reflectance. The spectral slope values were used to generate the gray scale maps of the light scattering index of the spinal cord near left L5.

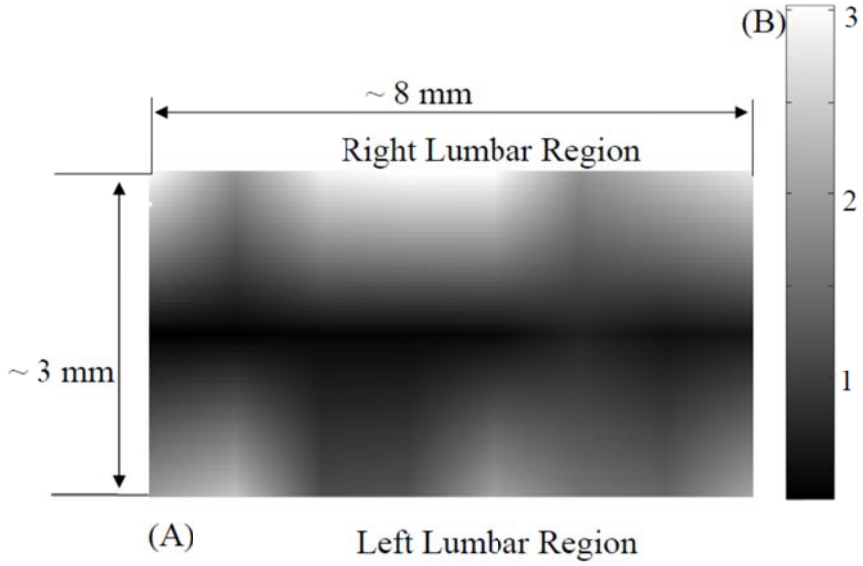

Figure 1.4 (A) A spectral-slope map with its gray scale bar (B) to show differences in spectral slope of the rat spinal cord [9].

As seen from Figure 1.4, the dark region represents lower slope values (0.34 to 0.67) at the center due to the presence of blood vessels. The lighter regions are the values with larger slopes (1.12 and 3.02) which represents the lumbar region of the spinal cord. The reduced scattering co-efficient, μ_s' was calculated using an algorithm developed by Johns et al., for needle-probe based measurements. According to the algorithm, for a range of μ_s' values between 5 to 60cm^{-1} and refractive index 'n' = 1.38, the relationship between μ_s' and the measured reflectance data taken with a 100μm separation can be approximated by

$$R = a_0 \, X \, (1.6696 \, X \, \mu_s' - \, 1.5437) \tag{1.1}$$

where,

R: measured reflectance

a_0: intensity factor calibrated from the experiments

μ_s': reduced scattering co-efficient in cm^{-1}

Table 1.1 Average Values of Slope of Spinal Cord [9]

No:	Left Lumbar	Blood Vessel	Right Lumbar
1	0.830	0.477	0.809
2	1.069	0.808	1.770
3	1.129	0.562	1.163
4	1.118	0.773	1.016
5	1.451	0.867	1.305
6	1.704	0.463	2.597
7	0.888	0.368	1.448
8	1.309	0.452	1.568
9	1.003	0.571	1.055
10	2.425	0.987	1.990
11	2.258	0.352	1.644
12	0.816	0.247	0.501
13	1.244	0.272	1.563
14	2.771	0.480	2.054
Mean	**1.430**	**0.549**	**1.463**
Std. Dev.	**0.628**	**0.228**	**0.547**

Table 1.2 Average Values of the μ_s' on the Spinal Cord Calculated using Equation 1.1 [9]

Sl No:	Left Lumbar	Blood Vessel	Right Lumbar
1	23.507	17.633	21.528
2	26.841	20.577	34.175
3	24.430	18.255	25.211
4	32.404	25.126	28.297
5	47.205	21.556	29.469
6	34.567	16.574	46.721
7	23.970	16.098	30.701
8	29.590	17.372	32.332
9	25.461	20.376	25.937
10	56.007	30.186	46.875
11	50.832	17.962	37.389
12	26.889	16.869	21.247
13	30.161	18.253	37.747
14	59.785	21.730	47.402
Mean	**35.118**	**19.898**	**33.216**
Std. Dev	**12.720**	**3.876**	**8.993**

Tables 1.1 and 1.2 represent the average values of slopes and μ_s' in the left and right lumbar and the central portion of the spinal cord for all fourteen rats. After analyzing the slope values for all fourteen rats the blood vessel region near the center shows a slope value of 0.55±0.23, while the rest of the mapped regions on either side of the central blood vessel have slope values ranging around 1.45±0.5.

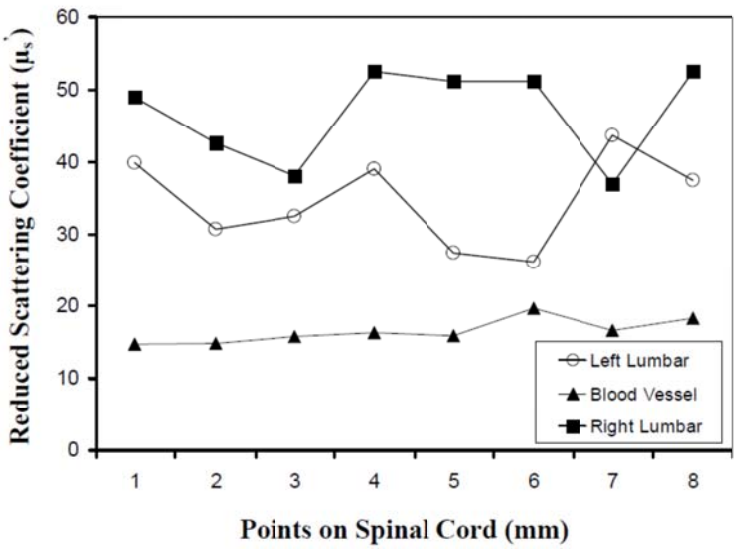

Figure 1.5 A plot to show variation in μ_s'. The values are from the left, right, and central lumbar regions of the spinal cord. The μ_s' values are computed at 750nm with the unit of cm^{-1} [9].

Figure 1.5 shows a plot of μ_s' values at 750nm from one rat, which is obtained using Equation 1.1. The study reported the μ_s' values of $32.2\pm2.1cm^{-1}$ and $19.9\pm1.0cm^{-1}$ for the lumbar regions and central region containing blood vessels respectively (see table 1.2). Thus, it was concluded that the spectral slope maps and the μ_s' maps of the rat spinal cord have been generated with higher μ_s' values in the lumbar regions ($34.2\pm2.1cm^{-1}$) and lower values at the center of cord ($19.9\pm1.0cm^{-1}$) near the blood vessels.

1.3 Introduction to Optical Techniques

C. Giller developed an optical stereotactic probe employing near-infrared (NIR) spectroscopy to provide intraoperative localization by distinguishing gray matter from white matter [10]. Figure 1.6 describes the operation of NIR probe used by C. Giller to determine the optical properties of brain tissues. He directed white light through a stereotactic probe which is scattered by tissue at the probe tip. Scattered light is conveyed

to a spectrometer to produce a graph of reflectance versus wavelength. The trailing slope of this graph is used as a reflectance index[10].

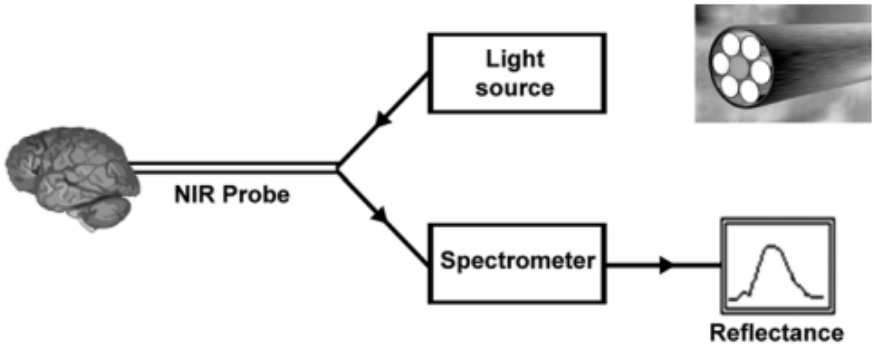

Figure 1.6 Schematic arrangement of NIR equipment [10].

When light propagates within tissue, it undergoes multiple elastic scattering and absorption depending on tissue optical properties. The prominent properties are the scattering coefficient of the tissue, μ_s, and the absorption coefficient of the tissue, μ_a. In the near infrared region, light scattering is more prominent than light absorption [9]. This is because the mean scattering free path ($1/\mu_s$) of tissue for near-infrared light is on the order of 10-100 microns while the mean absorption free path ($1/\mu_a$) is much longer. Anisotropy (g) is a measure of the amount of forward direction retained after a single scattering event. If a photon is scattered by a particle and deflected by an angle θ, the component of new trajectory aligned in the forward direction is given by cos(θ). Therefore, an average deflection angle and the mean value of cos(θ) is defined as anisotropy, i.e., g = cos(θ). The two limiting cases are g = 0 for ideal isotropic scattering, and g =1 for complete forward scattering of the incident beam. The reduced scattering coefficient (μ_s') is defined as

$$\mu_s' = (1-g)\mu_s \tag{1.2}$$

1.3.1 Direct Method

Two techniques have primarily been used to measure the optical properties of biological tissues; direct and indirect methods [11]. Direct method is based on Beer's law where a thin piece of tissue is used, for instance, as in the collimated transmission technique. In this method, the unscattered transmitted light is detected and penetration depth is calculated according to Beer's law (Figure 1.7).

Beer's law can be expressed as

$$It = Io \times (1 - R) \times e^{\frac{-x}{a}} \tag{1.3}$$

where,

It: transmitted light energy

Io: incident light energy

R: reflection coefficient of the surface

a: penetration depth. Penetration depth is defined as the distance at which the total optical power is reduced to 37% of the incident light.

The scattering coefficient is predicted from experimental measurements of light intensity and reflectance together [12].

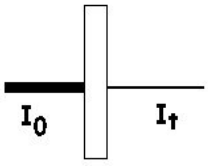

Figure 1.7 Diagram of Beer's absorption of a beam of light as it travels through a thickness of material [9].

1.3.2 Indirect Method

Indirect method is based on a model of light transport. The integrating sphere method is a common technique where the absorption coefficient (μ_a) and the reduced scattering coefficient (μ_s') are deduced from measurements of diffuse reflectance and total light intensity. The coefficients are then predicted based on light transport models such as the Monte Carlo method [13].

CHAPTER 2

METHODS

2.1 Fiber Optic Probe

Fiber optic sensors have attracted more and more attentions with the development of modern measurement technologies. Use of optical fibers for light measurement offers key mechanical benefits regarding device size and flexibility [14]. However, the main advantage of using a fiber optic cable is its vast bandwidth. This bandwidth is known to be much higher than the bandwidth of all studied electronic detection and processing techniques [15].

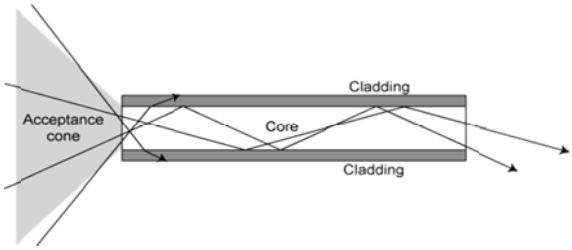

Figure 2.1 The structure of an optical fiber showing internal reflection [16].

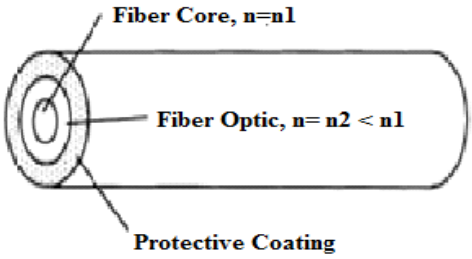

Figure 2.2 Difference in the refractive index of fiber optic and cladding [17].

An optical fiber is a glass fiber with a cylindrical core surrounded by a concentric cladding (Figure 2.1). The refractive index of the cladding is lower than that of the core (Figure 2.2). When light is sent into the core at a low angle, total internal reflection takes place and the light signal will be transmitted along the fiber with very little loss (Figure 2.1).With an optical fiber, signal can therefore be transmitted over very long distances without the need for amplification. To protect the optical fiber against scratches and environmental attack, a coating is always applied onto the fiber during the drawing

process. In most cases, the coating is made of a polymer (such as acrylate or polyimide). For special applications, a metallic coating such as aluminum or gold can be employed.

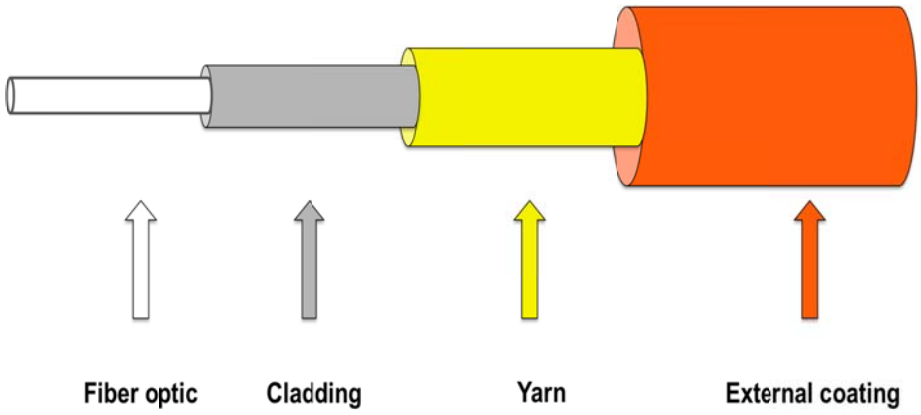

Figure 2.3 Schematic representation of Ø120µm sized fiber optic.

AMP NETCONNECT (catalogue # E92128) is a glass optical fiber used during the experiment to measure the light intensity from the laser. It is a multi mode simplex non-conductive riser fiber optic having diameter of 120µm [18]. The fiber optic is chosen such that it transmits light even in the NIR range which is the spectrum of interest. It has a maximum attenuation of 3dB/km @ 850nm and maximum attenuation of 1.25dB/km @ 1300nm [18].

2.1.1 Fiber Optic Preparation

As shown in Figure 2.3, the fiber optic is covered with two layers of protective coatings and a layer of cladding. For this study, approximately 4-5cm of bare fiber optic was used. It was chosen such that to cause least possible damage to the surrounding tissues during insertion. The total length of the entire fiber optic assembly was around 4ft. and during each experiment appropriate length of fiber optic was prepared using a combination of surgical blade, micro sandpapers and a standard wire stripper. The tip of the fiber optic

was polished using three different sizes of micro sand papers starting from largest to the smallest. The fiber optic was polished to have a uniform cross sectional area for the incident light. The two coatings and the cladding were removed using a surgical blade and a wire stripper.

2.2 NIR Laser Source

A NIR laser source, DLS-500-830FS-100 manufactured by StockerYale, Canada was used in our experiment [19]. It is a laser diode that has a wavelength of 830nm and has a maximum peak power of 73.8mW. Since the beam operates at a fundamental transverse electromagnetic mode [TEM_{00}] it has a Gaussian profile and a circular footprint [20]. The Gaussian profile is crucial for this experiment as it gives lower beam divergence and a good spatial coherence. This means that the beam can be focused to a smaller spot.

The Gaussian function is of the form

$$f(x) = ae^{-(x-b)^2/c^2} \tag{2.2}$$

where,

a: the amplitude

c: the standard deviation

x: variable

b: constant value

Here the transverse profile of the optical intensity (I) of the beam with a power *P* can be described with a Gaussian function as

$$I(r) = \frac{P}{\pi w^2/2} e^{\left(\frac{-2r^2}{w^2}\right)} \tag{2.3}$$

where,

r: the distance from the center of the beam and is measured in polar co-ordinates

w: the spot size of the Gaussian beam or the Gaussian beam radius where the intensity drops to $1/e^2$ (≈ 13.5%) of the maximum value.

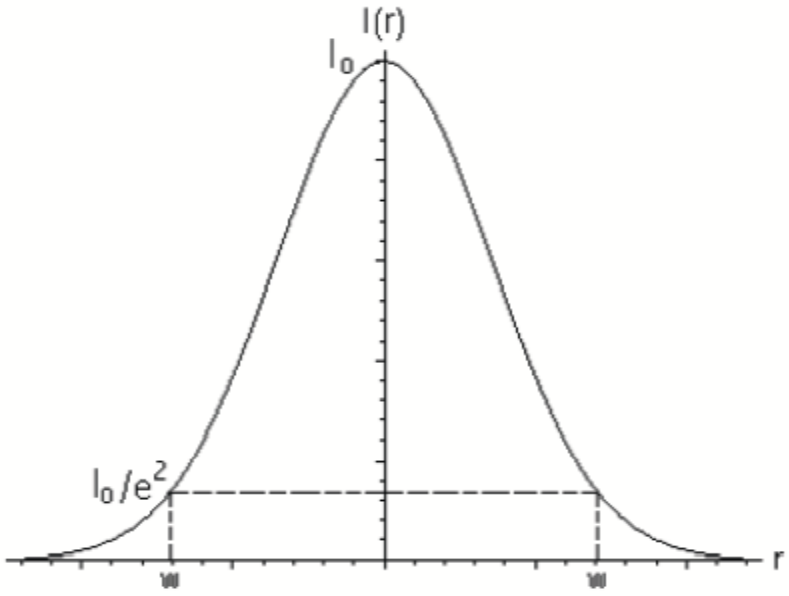

Figure 2.4 Laser beam having a Gaussian profile [20].

The spot size w is a function of z, i.e., the direction in which the wave is propagating and will be at a minimum value w_0 at a specific point along the beam axis, known as the beam waist. For a beam of wavelength λ [21]

$$w(z) = w_0\sqrt{1 + (\frac{z}{z_R})^2} \tag{2.4}$$

where z_R is given as

$$\text{Rayleigh range, } z_R = \frac{\pi {w_0}^2}{\lambda} \tag{2.5}$$

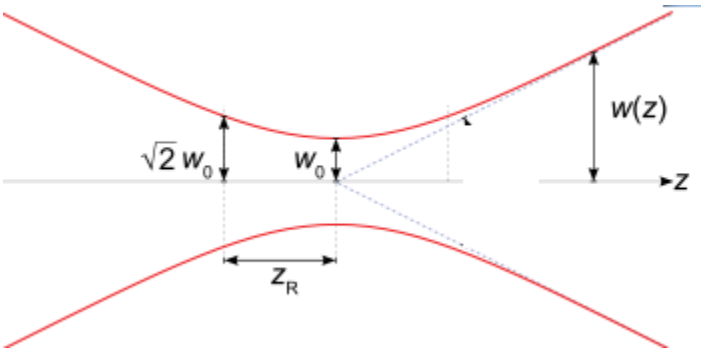

Figure 2.5 Gaussian beam width $w(z)$ as a function of the axial distance z. w_0: beam waist; b: depth of focus [19].

2.2.1 Laser Calibration

Laser was calibrated to determine the amount of power produced for a given range of DC control voltage. The laser was modulated with voltages from 0V to 4.5V in steps of 50mV and changes in the power were recorded [22]. The light from the laser was incident on the fiber optic described in Section 2.1 which was connected to a photodiode. The photodiode produced an electric current corresponding to the incident laser beam power. The current from the photodiode was passed through a current to voltage converter (Figure 2.9) and using Equations 2.4 and 2.5 for an 830nm laser when it is at a distance of 13.5cm from the optic the spot size is 0.56mm [20]. The power of the laser is given by

$$P = \frac{I}{R} \tag{2.6}$$

where,

P: Light power (mW)

I: Photodiode current (mA)

R: Responsivity of the photodiode (mA/mW)

Average power density is given by

$$P.D = \frac{P}{A}\ X\ PW\ X\ f \tag{2.7}$$

where,

A: Cross-sectional area of the beam at target (cm^2)

PW: pulse width (s)

f: frequency (Hz)

The product $PW\ X\ f$ is the called the duty cycle.

Figures 2.6 and 2.7 show photodiode's current output in the path of laser light as a function of laser control voltage. As seen from Figure 2.6 when the laser modulation voltage is increased from 0V to 4.5V the photodiode current reduces linearly from 1.1mA to 0mA. A fourth order polynomial curve was fitted to the data using the least squares method. Equation 2.6 was used to calculate the corresponding power which was plotted against the modulation voltage. Figure 3.7 shows that there is a linear correlation of R^2 = 0.99 between power and control voltage of NIR laser. The output power decreases with the increase in input voltage. The input-output relation was described by y = 3.4594 x – 0.1863 where x is the control voltage in volts and y is the laser power in mW/mm^2.

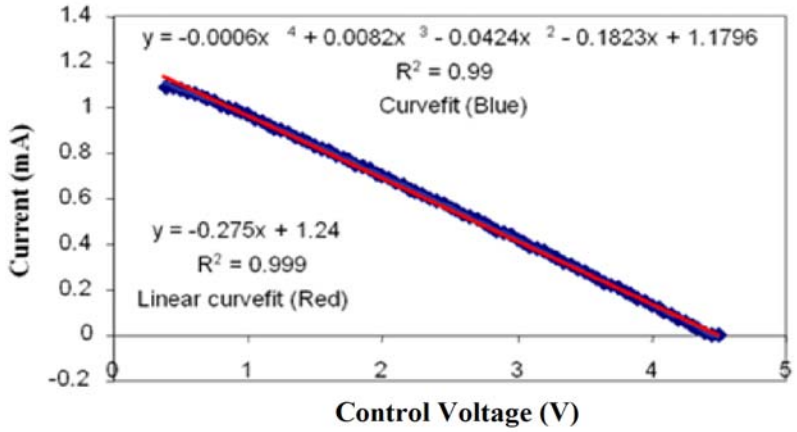

Figure 2.6 Laser's current output versus control voltage. Percent error in curve fit = 0.79% [22].

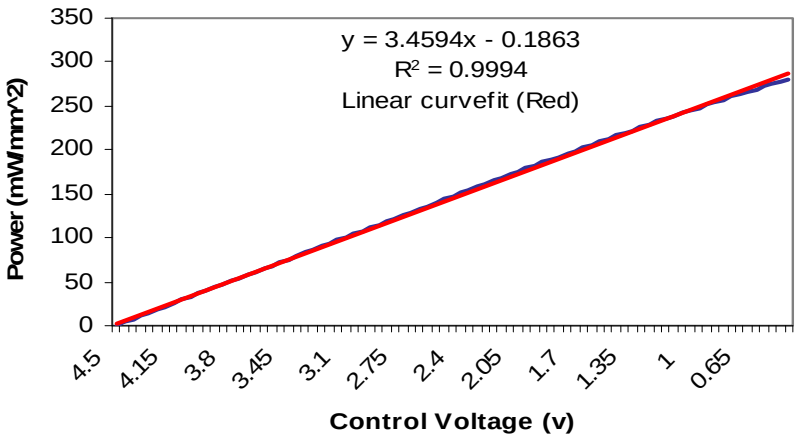

Figure 2.7 Laser's power output versus control voltage [22].

2.3 Animal Preparation

Five Sprague-Dawley rats (250-300g) were used for this study but only data from two animals had sufficient stability to report in this thesis. A mixture of ketamine (80mg/kg) and xylazine (12mg/kg) diluted with saline was injected intraperitorially for anesthesia. The heart rate (HR) was monitored continuously using a neonatal pulse oximeter. A sudden increase in the HR indicated the diminishing effect of anesthesia and further doses of ketamine were administered. The reflexes of the lower limbs were also checked periodically for signs of arousal from anesthesia. Marcaine (0.2ml) was injected at the site of incision as a local anesthetic. Dexamethasone (2mg/kg) was administered intramuscularly at the beginning of the surgical procedure to prevent edema in the central nervous system. The rectal temperature was continuously monitored and maintained between 35-36^{o}C using a temperature regulated heating pad. Dehydration of brain tissue was prevented using a pool of warm saline over the exposed area of the brain. All procedures were approved and performed in accordance with the guidelines of the Animal Care and Use Committee, Rutgers University, Newark, NJ.

2.4 Data Acquisition Interface

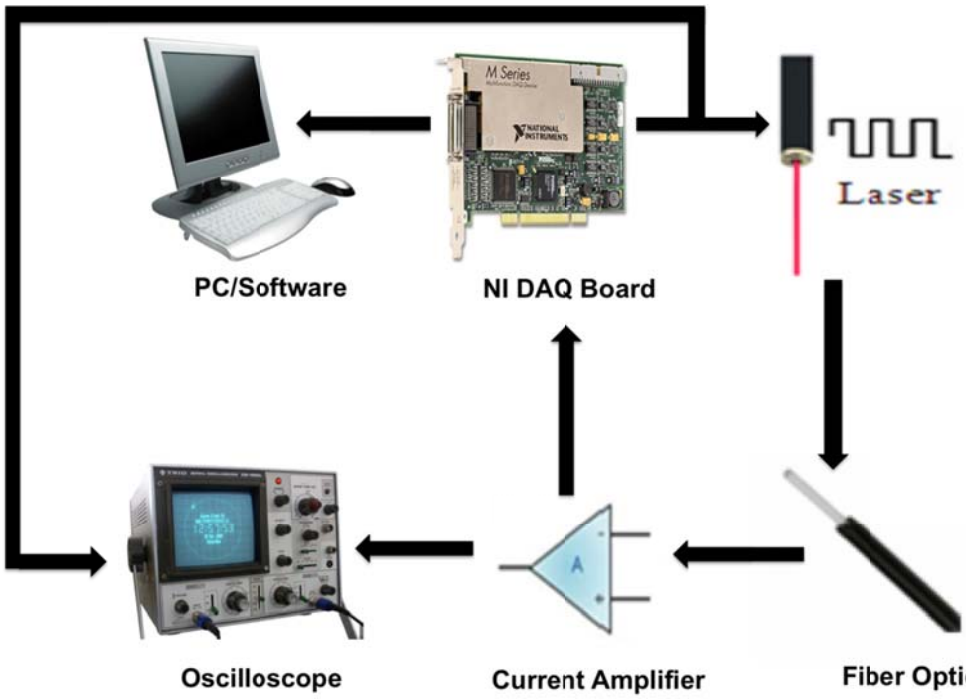

Figure 2.8 Block diagram of interfacing of the computer with the electronic circuit, laser and the fiber optic.

As seen from Figure 2.8, the laser output is controlled via custom MATLAB software through the National Instruments (NI) Data Acquisitions (DAQ) board. The output from the photodiode of the fiber optic is given to a current amplifier. The output of the current amplifier is fed to the computer through the DAQ board for recording. The outputs from the DAQ board and the current amplifier are also connected to the two channels of the oscilloscope to see any instantaneous change in the signal.

2.4.1 Software

Custom MATLAB software was written as a part of a Master's thesis at NJIT to control the Laser output and record the input signal [23]. As seen from Figure 2.9 this software can be used to control the train parameters, frame parameters, signal modulation and recording parameters. Using the train parameters like the pulse frequency, pulse width

and train duration, the input voltage can be controlled and trial number, recording time, sampling rate and min/max input range controls the signal from the fiber optic. This software also gives an option to show live plots of the signal and to save the data for future analysis.

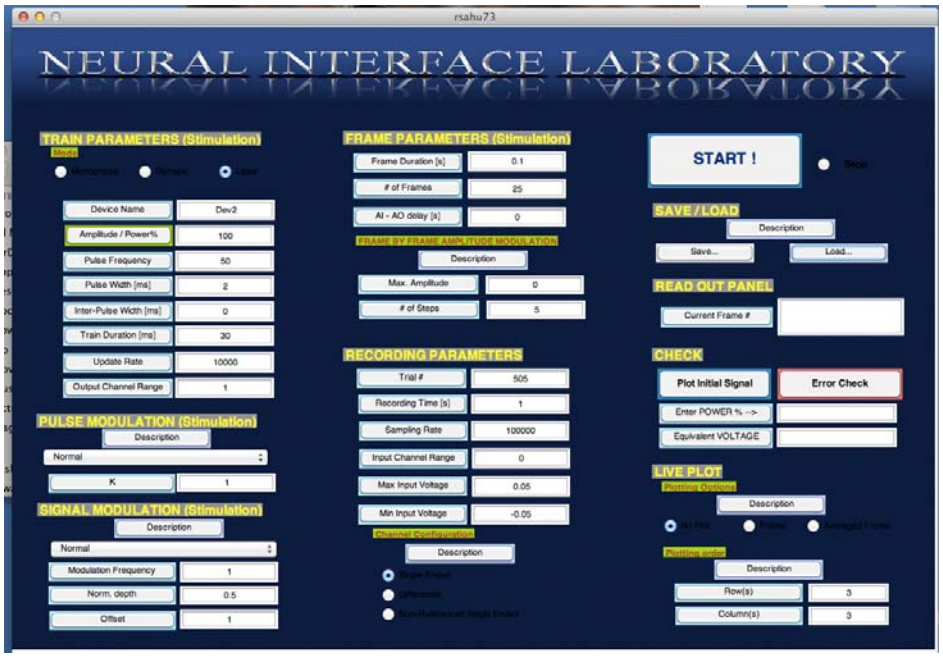

Figure 2.9 Custom Matlab software user interface [23].

2.4.2 National Instruments Data Acquisition (NI DAQ) Board [24]

NI PCI 6259 DAQ Board was used in this study. It is a high speed DAQ board with sampling rates upto 1.25MS/s. It has four 16-bit analog outputs, 48 digital I/O and 32-bit counters. However, only one analog input and output and one digital input & output were used in this study. The analog output from the DAQ board controlled the laser power. The signal from the fiber optic and through the amplifier is applied to the DAQ board, which digitized it and sent it to the computer for saving on the hard disk.

2.4.3 Current Amplifier

A current amplifier circuit was used between fiber optic output and NI DAQ board to convert the photodiode current into voltage. The use of a current amplifier ensures that the photodiode output voltage is zero hence the current is transferred to the amplifier without a loss. The Op-amp circuit is a current amplifier with the value of R1 as 200kΩ and 5kΩ for the first and second experiment respectively. The schematic of circuit is shown in Figure 2.10.

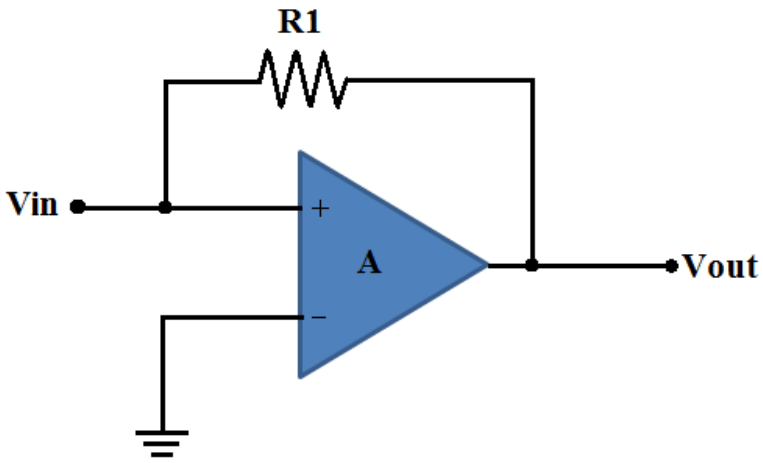

Figure 2.10 The current amplifier.

2.5 Surgery

The experiment was performed using two 250-300g Sprague- Dawley rats. Anesthesia was induced as described in Section 2.3 and the head was immobilized using a stereotaxic frame. A 4x6mm cranial opening was made rostral to the Bregma on the right side of the central fissure (Figure 2.11). The dura mater was removed. Dehydration of brain tissue was prevented using a pool of saline.

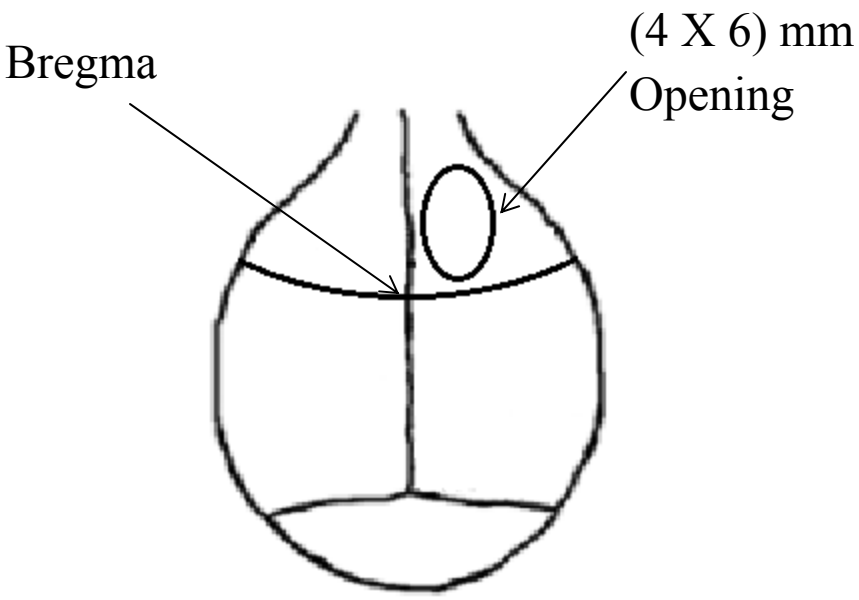

Figure 2.11 Exposed area of the cerebral cortex for light measurements in the experimental animals [20].

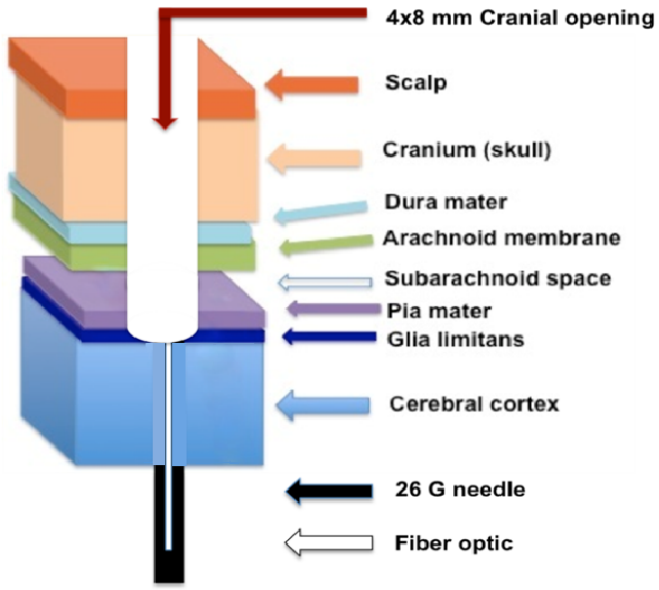

Figure 2.12 Schematic representation of fiber optic into the cerebral cortex.

A 25G needle was slowly inserted into the brain through the base of the skull, by avoiding major vessels, until it reached the cortical surface ~1mm rostral and ~1mm lateral to the Bregma through the skull opening as shown in Figure 2.12. An optical fiber

(Ø120µm, AMP NETCONNECT) was attached to a micromanipulator and inserted through the needle from the lower end until its tip was leveled with the cortical surface as shown in Figure 2.13.

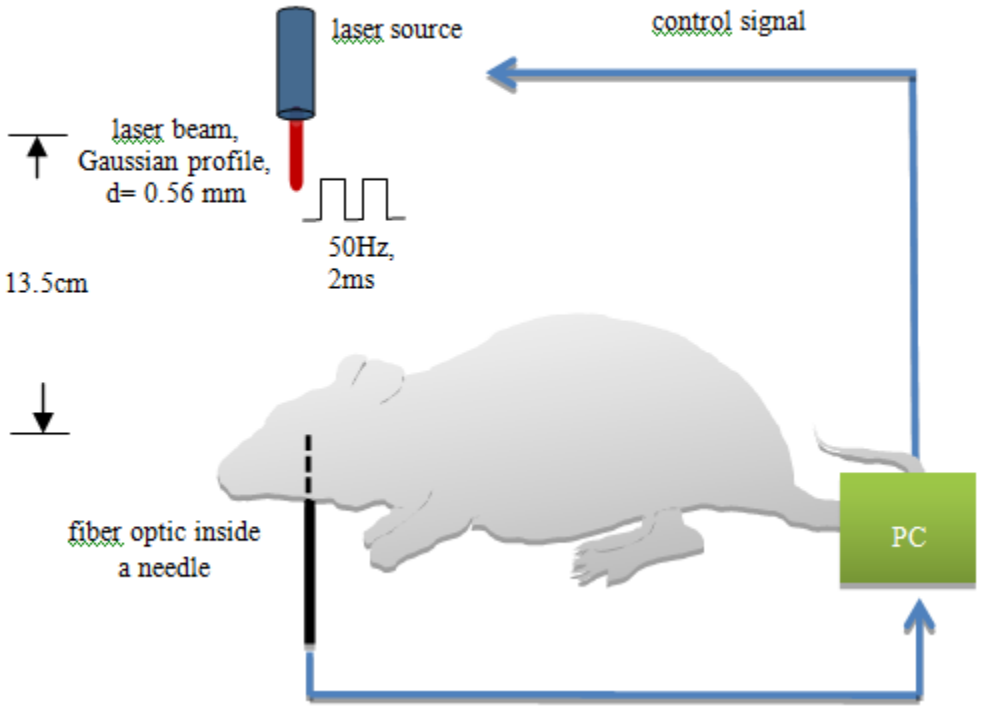

Figure 2.13 Sketch of the preparation used to measure the light intensity due to light radiation in the rat brain.

The laser was placed 13.5cm above the brain using another micromanipulator and aimed at the fiber from above (Figure 2.13). The laser source and acquisition of the signals into the computer were controlled by a MATLAB code. A train of NIR pulses were sent to the fiber with a circular footprint of 0.56mm in diameter at the cortex. Vertical displacements of the probe were controlled by moving 1-axis micromanipulator into the tissue as mentioned above, therefore making measurements in a 2D vertical plane sagittally oriented. The light intensity was measured at different depths (250-1500µm in steps of 250µm). For each depth of the fiber position, the laser beam was horizontally

moved by 600μm from the origin in steps of 125μm while taking measurements at each step.

CHAPTER 3

RESULTS AND DISCUSSION

3.1 Experimental Results

Figure 3.1 depicts an example of light intensity signal recorded during the second experiment at a depth of 625µm and 500µm horizontally from the central position of the pia matter surface. The signal is measured in terms of its equivalent voltage by passing it through a current amplifier having a resistance of 200kΩ and sampled at a sampling frequency of 100kHz. The variation of the peaks is due to the breathing motion of the rat.

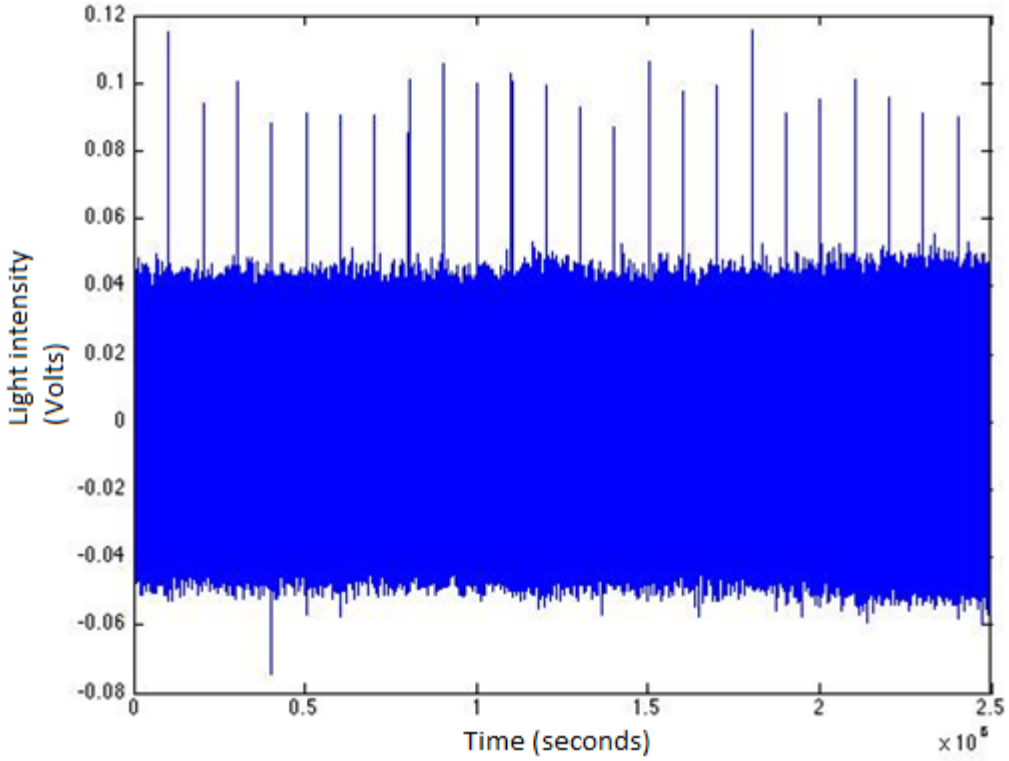

Figure 3.1 Raw light intensity signal at 625 by 500µm (depth and horizontal displacement). The output of the current amplifier is shown in the plot.

This signal was then filtered using a second order low pass butterworth filter to eliminate the noise. Figure 3.2 represents a filtered version of Figure 3.1.

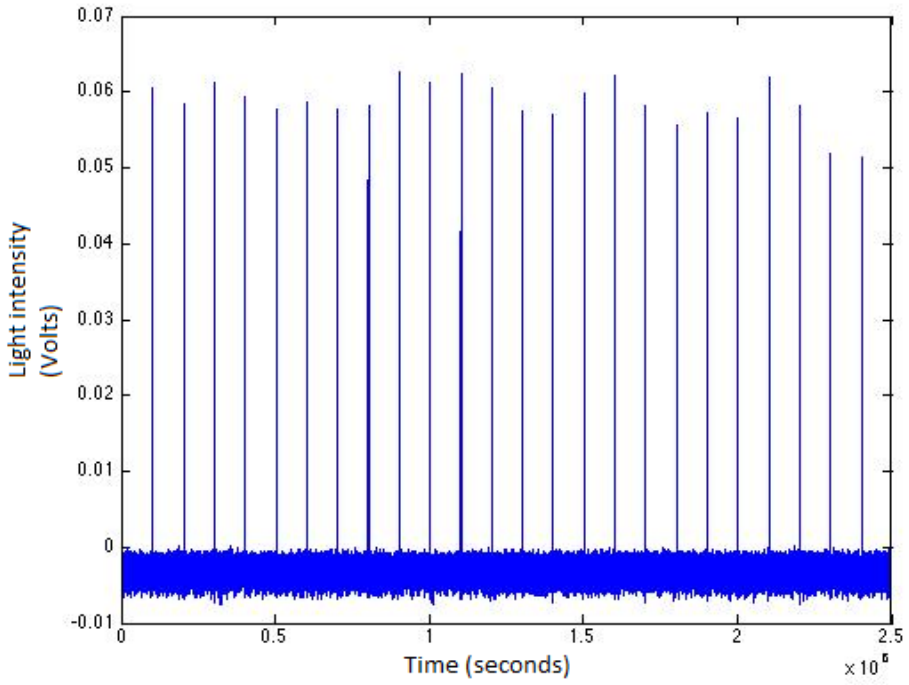

Figure 3.2 Filtered light intensity signal shown in Figure 3.1.

The data was averaged to get the mean for each pulse train. The equivalent current was then calculated by dividing the mean with the resistor in the current amplifier. Tables 3.1 and 3.2 summarize the mean, current and light intensity values for displacements in the horizontal directions up to 625μm and for depths up to 1500μm.

Table 3.1 Summary of NIR Intensity in terms of Voltage, Current and Light Intensity during the 1st experiment.

Resistance=200kΩ

Horizontal Displacement (µm)	Voltage (Volts)	Current (µA)	Light intensity (%)
Depth=250µm			
-125	3.608	18	100.00
0	7.5401	37.7	209.44
125	1.6595	8.3	46.11
250	0.6029	3.01	16.72
375	0.1342	0.671	3.73
500	0.0341	0.171	0.95
Depth=500µm			
-125	1.8323	9.16	50.89
0	5.964	29.8	165.56
125	2.0165	10.1	56.11
250	0.8875	4.44	24.67
375	0.2893	1.45	8.06
500	0.0549	0.275	1.53
Depth 750µm			
-125	1.6878	8.44	46.89
0	2.9237	14.6	81.11
125	2.3702	11.9	66.11
250	1.1687	5.84	32.44
375	0.3836	1.92	10.67
500	0.1251	0.626	3.48
Depth=1000µm			
-125	0.3205	1.6	8.89
0	0.446	2.23	12.39
125	0.5259	2.63	14.61
250	0.4824	2.41	13.39
375	0.3614	1.81	10.06
500	0.2421	1.21	6.72
Depth=1250µm			
-125	0.1887	0.944	5.24
0	0.145	0.725	4.03
125	0.2485	1.24	6.89
250	0.2304	1.15	6.39
375	0.2376	1.19	6.61
500	0.2649	1.32	7.33
Depth=1500µm			
-125	0.171	0.855	4.75
0	0.1531	0.76	4.22
125	0.1205	0.603	3.35
250	0.0895	0.448	2.49
375	0.0662	0.331	1.84
500	0.0494	0.247	1.37

Table 3.2 Summary of NIR Intensity in terms of Voltage, Current and Light Intensity during the 2nd experiment.

Resistance=5kΩ

Horizontal Displacement (µm)	Voltage (Volts)	Current (µA)	Light Intensity (%)
Depth= 250µm			
0	0.1215	24.3	100.00
125	0.1146	22.9	94.24
250	0.153	30.6	125.93
375	0.1622	32.4	133.33
500	0.0578	11.6	47.74
625	0.0401	8.02	33.00
Depth= 500µm			
0	0.0509	10.2	41.98
125	0.0641	12.8	52.67
250	0.153	30.6	125.93
375	0.0816	16.3	67.08
500	0.0438	8.76	36.05
625	0.0105	2.1	8.64
Depth= 750µm			
0	0.0509	10.2	41.98
125	0.1146	22.9	94.24
250	0.0452	9.04	37.20
375	0.0524	10.5	43.21
500	0.0302	6.04	24.86
625	0.0264	5.28	21.73
Depth= 1000µm			
0	0.138	27.6	113.58
125	0.0173	3.46	14.24
250	0.0215	4.3	17.70
375	0.0282	5.64	23.21
500	0.0173	3.46	14.24
625	0.0182	3.64	14.98
Depth= 1250µm			
0	0.0072	1.44	5.93
125	0.0093	1.86	7.65
250	0.0099	1.98	8.15
375	0.0139	2.78	11.44
500	0.0093	1.86	7.65
625	0.0105	2.1	8.64
Depth= 1500µm			
0	0.0044	0.88	3.62
125	0.0059	1.18	4.86
250	0.0055	1.1	4.53
375	0.0075	1.5	6.17
500	0.0061	1.22	5.02
625	0.006	1.2	4.94

Using the data in Tables 3.1 and 3.2 the light intensity curve was plotted for different horizontal displacements of the laser beam by 625µm from the origin in steps of 125µm as a function of depth. Figures 3.3-3.8 represents the NIR intensity inside the brain as a function of depth for different horizontal displacements of the laser beam. Each plot is normalized by its intensity measurement at a corresponding point at the cortical surface.

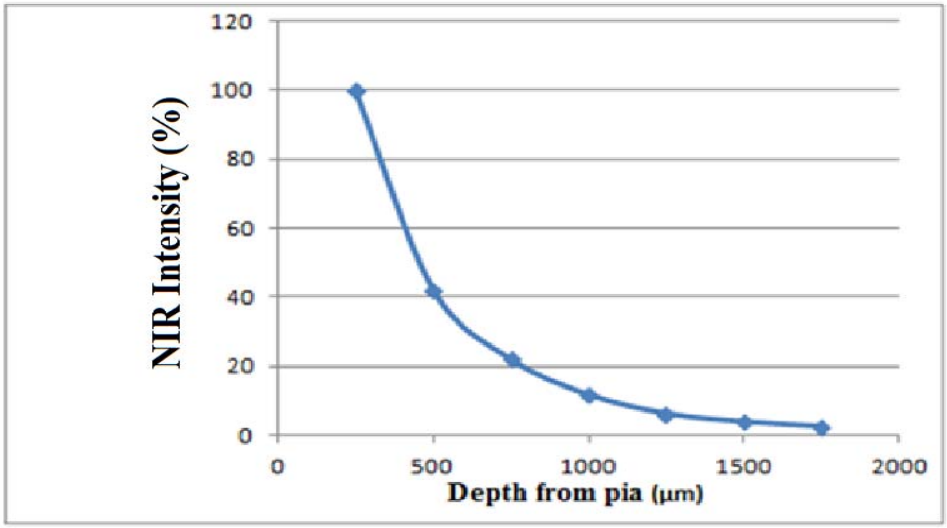

Figure 3.3 Light intensity curve when the laser beam is at central location.

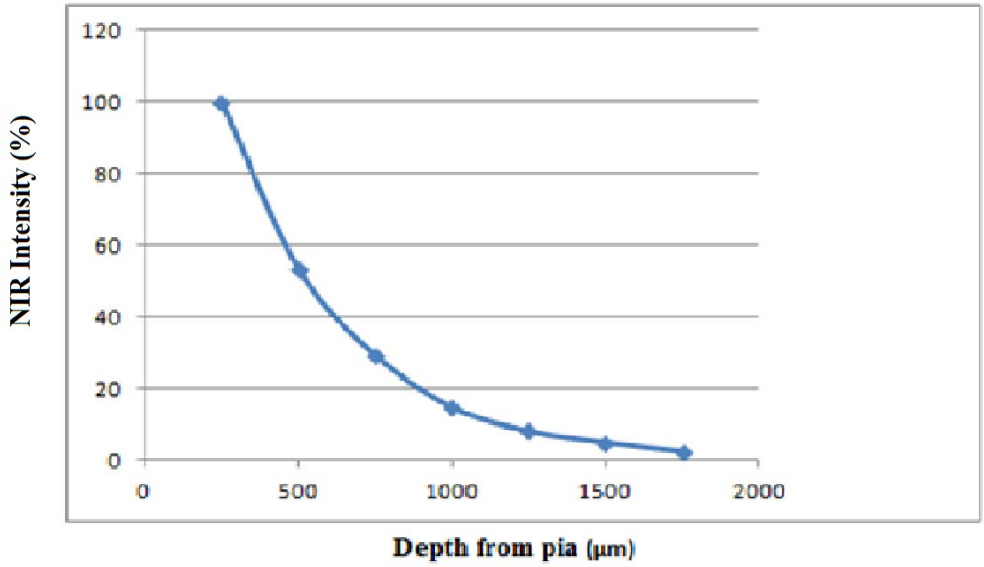

Figure 3.4 Light intensity curve when the laser beam is at 125µm from center.

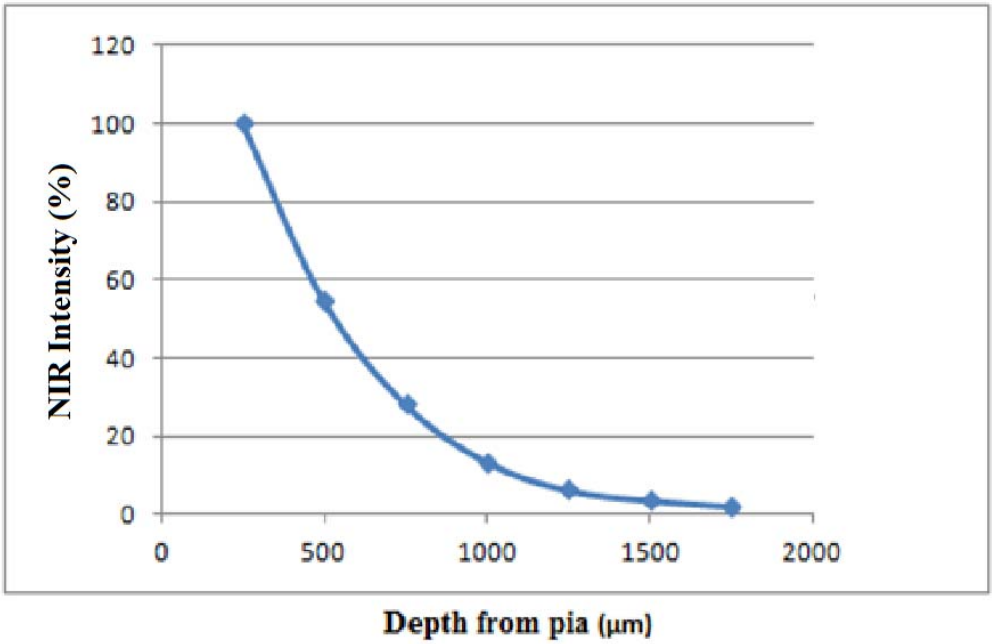

Figure 3.5 Light intensity curve when the laser beam is at 250μm from center.

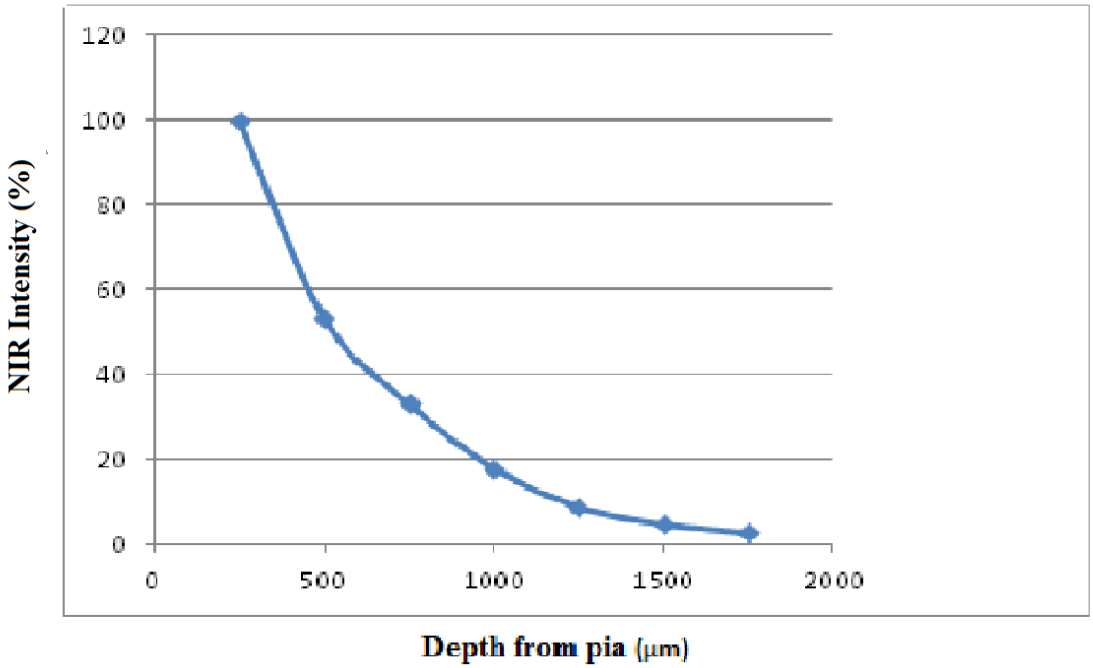

Figure 3.6 Light intensity curve when the laser beam is at 375μm from center.

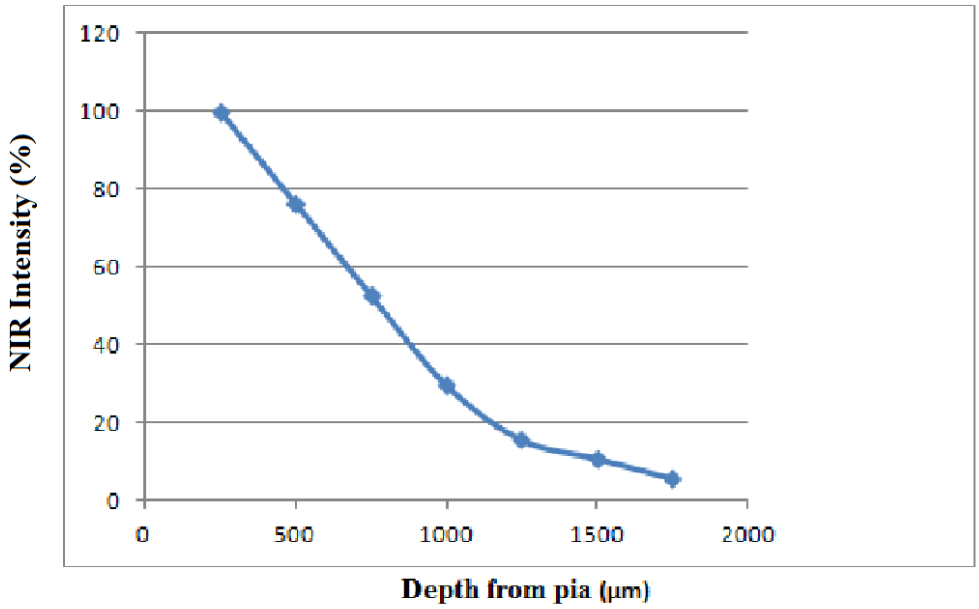

Figure 3.7 Light intensity curve when the laser beam is at 500µm from center.

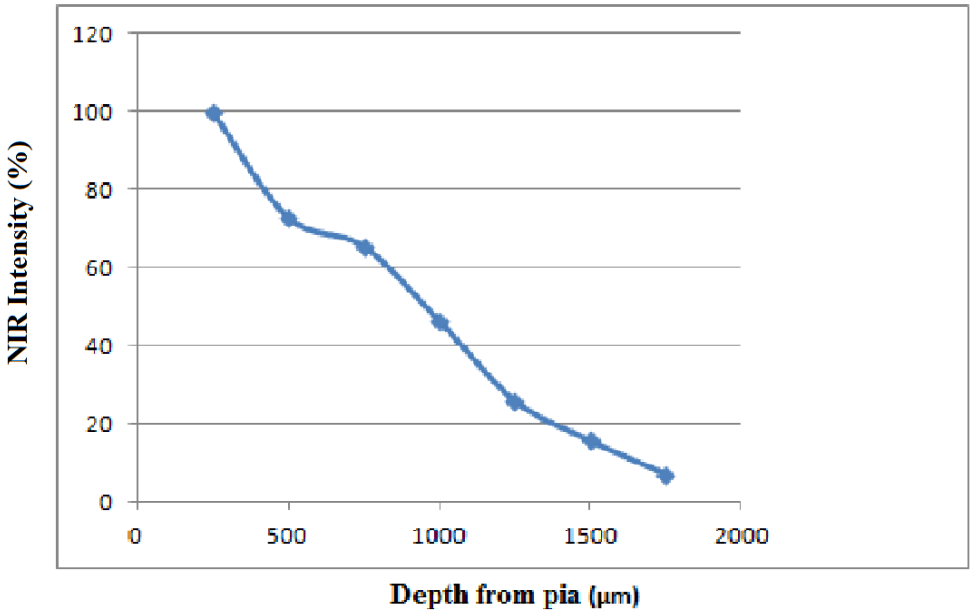

Figure 3.8 Light intensity curve when the laser beam is at 625µm from center.

Figure 3.9 shows the average NIR intensity of the two experiments inside the brain as a function of depth at the center of the laser beam. The mean values were 56%, 40%, 26%, 7%, 3%, and 2% at depths of 250, 500, 750, 1000, 1250 and 1500µm

respectively. The data in Figure 3.9 predicts a steady rate of decrease in light intensity up to 1000µm and then a slower rate of decrease afterwards.

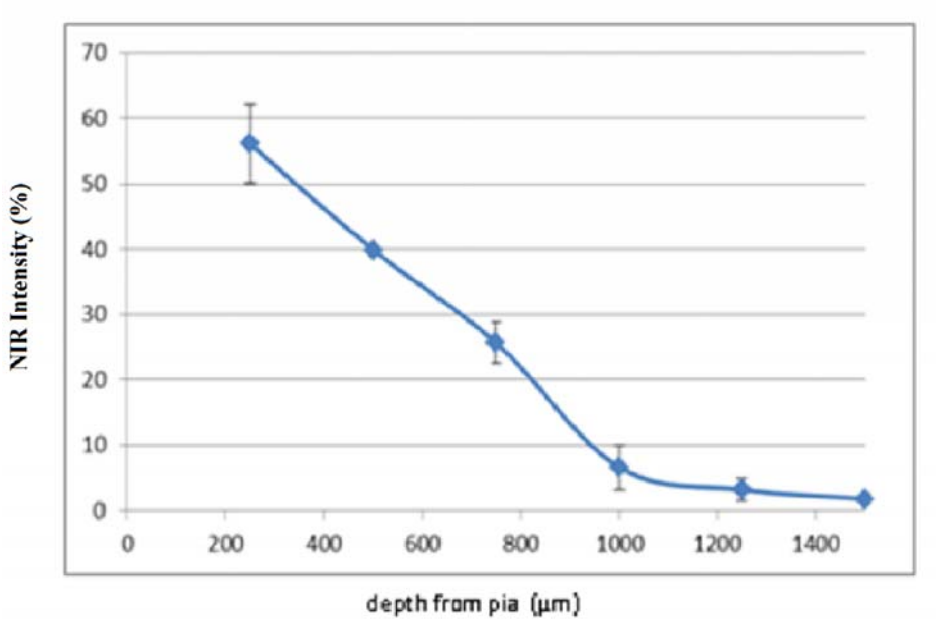

Figure 3.9 The average light intensity measurements in two animals as a function of depth in the rat brain gray matter.

Figure 3.10 shows the 2D map of light intensity within the vertical half plane in the rostro-caudal direction. In the horizontal direction, the light intensity profile drops quickly almost following the same course as the laser intensity curve. However, it extends a few times the laser diameter in the vertical direction. Measurements were made in steps of 250µm in the vertical and 125µm in the horizontal directions and then interpolated for intermediate points. The light intensities are normalized by the light intensity at the pial surface in the beam center. Note that vertical and horizontal axes are not on the same scale. The bell shaped curve in Figure 3.10 shows the laser intensity profile aligned with respect to the 2D temperature plot. The white area indicates the

superficial layers of the cortex where the measurements had a large variation, and thus not included in the plots.

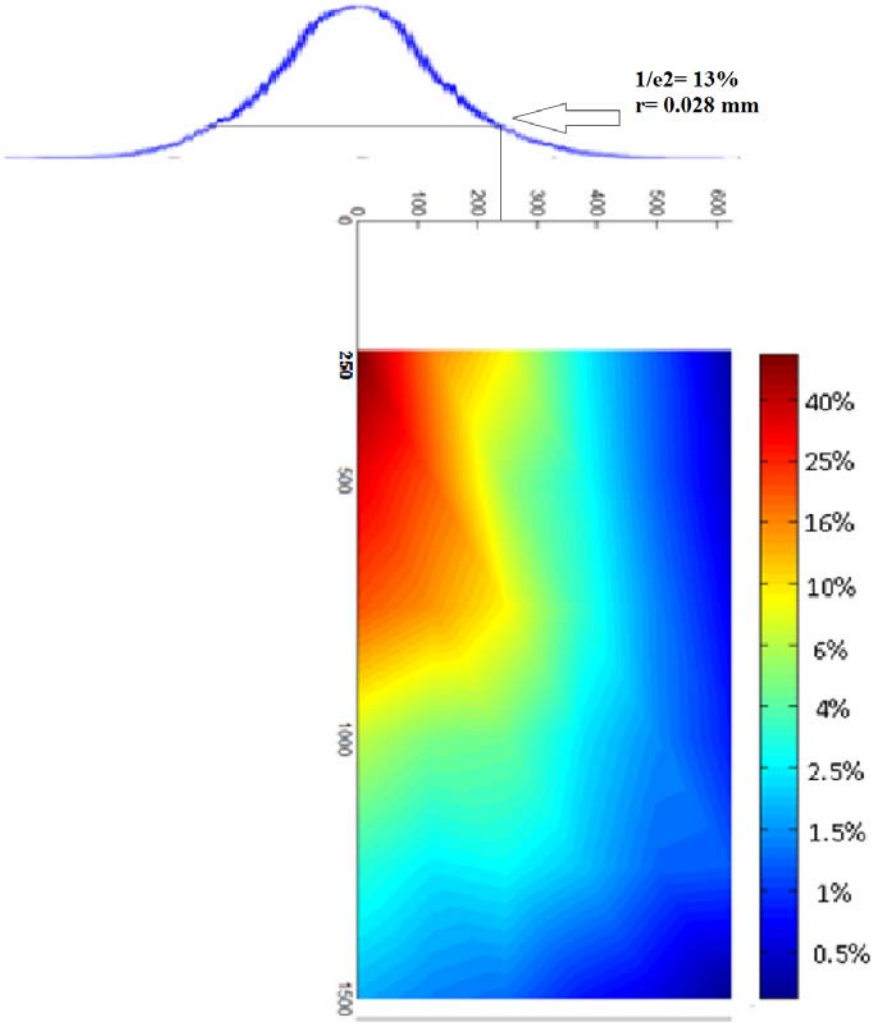

Figure 3.10 2D illumination inside the rat brain due to a total laser power of 74mW. The light intensities are shown in logarithmic scale as a percentage of the maximum value at (0, 0) point.

3.2 Discussion

Optical properties of neural tissue play an important role. NIR Laser light can penetrate with more ease into neural tissue than visible light. The dominant form of interaction with the neural tissue at NIR wavelength is scattering [11]. Since grey matter has lower

scattering coefficient than white matter, NIR light penetrates more readily into the grey matter [6, 8].

This study reports the spatial distribution of photons inside the rat brain gray matter while being radiated by a beam of NIR laser. As seen from Figures 3.5- 3.10 there is an exponential decrease in photon density by depth into the neural tissue. Tables 3.1 and 3.2 tabulate the numerical values. These results are consistent with the available *in vitro* data [3, 8, 9]. The outliers in the light intensity values are mainly due to the mechanical limitations in measuring the light intensities. The mean light intensity of the gray matter shown in Figure 3.11 is in agreement with the *in vitro* data measured in unfrozen samples of rat brain gray matter [8]. Some reports in literature suggest that *in vitro* measurements of optical properties can adequately match the *in vivo* case if appropriate precautions are taken [4].

Figure 3.12 represents the 2D spatial distribution of light photons in the neural tissue giving rise to a bell shaped curve. As predicted the maximum amount of light intensity is at the center and at a depth of 250μm. As the beam deviates from the central position the light intensity falls and is around 0.5% at 625μm. This effect is justified by Gaussian shape of the laser beam. As the light penetrates deeper into the tissue the light intensity falls to around 10% at a depth of 1000μm. This is mainly due to the multiple scattering that takes place within the tissue and due to low scattering co-efficient of the gray matter. Overall, the light intensity decreases exponentially as a function of depth. The light intensity at a depth of 1000μm is around 10%. The same light intensity point (10%) in a horizontal direction occurs at around 250μm. Thus, the spatial gradient of light intensity decrease is steeper in the horizontal direction in comparison to the decline

in the vertical direction. In other words, NIR laser penetration is much stronger in the vertical direction than horizontal direction.

Sample preparation technique is very important in measurements of tissue optical properties. The data presented in this report are more realistic because the measurements were made in live animals. Roggan *et al.* found that both shock and slow freezing procedures alter the optical properties of biological tissue [25]. The freezing procedure changes the optical properties by damaging the tissue due to mechanical forces generated by ice crystals. Chan *et al.* observed that compressing the tissue between microscope slides also alters the optical properties [26].

3.3 Limitations

The measurements near the pial surface were not very consistent due to external disturbances. Moreover, motion artifacts due to breathing and beating of the heart may have contaminated the signal. Accidental puncture of any blood vessel caused bleeding which could have been one of the potential reasons for the inconsistent readings at the surface. Despite these disturbances, a certain level of reproducibility was achieved in the measurements.

The study was performed by moving the laser horizontally in steps of 125μm and by moving the fiber optic vertically in the steps of 250μm. A better spatial resolution can be obtained by taking measurements in smaller steps both horizontally and vertically. A smaller diameter fiber could also yield a better spatial resolution. Another advantage of using a smaller diameter fiber optic is that it would reduce damage to the surrounding tissues during insertion.

During one of the reference experiments, there was blood coagulation in the tissues. Blood coagulation is an important factor that needs to be considered while measuring the NIR beam intensity as it might change the optical properties of the brain tissues [4]. These changes can significantly influence the resulting distribution of the optical radiation within tissue, and consequently the outcome of therapeutic procedure. During the coagulation process, the effective penetration depth of light into the tissue decreases for all the tissues investigated [4]. Thus, if laser irradiation leads to the structural changes within the tissue, the changes in the light penetration depth should be accounted while planning the therapeutic procedure.

Other factors include anesthesia, mechanical setup and the surgical procedure. The use of continuous gas anesthesia can prevent the frequent doses of anesthesia and can provide a more uniform level of anesthesia. A robust mechanical setup could prevent small slippage of the fiber optic during vertical displacement of the fiber optic. Finally, by improving the surgical procedure the damage to the neighboring tissues can be reduced which would further improve the reproducibility of data in this study.

CHAPTER 4

CONCLUSION AND FUTURE WORK

4.1 Conclusion

The analysis of the results obtained in this study shows that data is in agreement with the values reported in the literature. The shape of the light intensity curve also matches closely with the *in vitro* results obtained previously [8]. The discrepancies as well as the variations within the values reported in the literature for selected brain tissue structures are most probably due to the different theoretical models and sample preparation techniques employed [2, 4, 11, 27].

The results clearly demonstrate that the maximum penetration of the NIR beam is in the center. Figure 3.12 shows that the spatial distribution of NIR light intensity has a bell shaped curve. Since the beam is entering the medium vertically and due to the anisotropic property of the neural tissue, the NIR light spatial gradient is direction dependent. The spatial gradient is much smaller vertically than horizontally, i.e., the beam penetrates more in the vertical direction than horizontally.

Beam radius is a critical factor in many NIR laser applications [28]. The total amount of exposure depends on the beam size. An increase in exposure can increase the temperature induced which can in turn cause permanent damage to the surrounding tissue. As seen from Equation 2.3, the beam intensity is a Gaussian function of distance. Also, light penetrates deeper into the tissue as the beam radius increases up to a certain value (Figure 1.2). Thus, larger beam sizes are preferable in order to minimize the total NIR exposure while maintaining a certain photon density at the deep targets. Similarly, if

small diameter beam is used, a large temperature peak can occur in the center of the beam. To prevent such a situation, optical microlenses can be used to eliminate the spatial peak effect.

4.2 Future Work

The use of NIR light in medicine has increased tremendously over the last twenty years. Better understanding of these applications can be obtained by studying the interactions between NIR light and neural tissue. In this study, the penetration of the NIR beam at various depths inside the gray matter was studied and its spatial distribution was plotted. Monte carlo simulations is a powerful mathematical tool that can be used to further validate the results obtained. Also, by using the curve fitting method the reduced scattering co-efficient μ_s' and scattering co-efficient μ_s of NIR can be calculated.

Temperature elevation profile inside the tissue is a critical factor in many NIR applications. A temperature elevation of 1°C causes fatal damage in neural tissue [29]. Thus, studying the relationship between the light penetration and temperature profile would be extremely beneficial for these laser applications.

Furthermore, a similar study can be conducted in other parts of the central nervous system like the white matter in the brain and the spinal cord. Thus, complete understanding of NIR light interaction with neural tissue can be obtained by interpreting these results and comparing them with published data.

APPENDIX

MATLAB CODE FOR FILTERING AND AVERAGING SIGNAL

1 Filtering Signal

This matlab file filters the raw signal using a second order low pass butterworth filter.

```
fc= 10000;                  %  corner frequency of the filter (in Hz)
fs= 1000;                   % sampling freq(in Hz)
fn= 2*fc/(fs);              % normalize the corner frequency with fs
[b,a]=butter (2, fn);       % design a 2nd order butterworth filter, low pass
f= filter (b, a, data);     % filters the raw signal
plot (f);                   % plots the filtered signal
```

2 Averaging Filtered Data

```
for i = 1: length (f)          % creates a loop of the length of filtered data
if f (i, 1) >= 0.015           % compares each value of the filtered data with pre set noise
                               amplitude
d (i,1) = f (i,1);             % if value of filtered data greater than 0.015, that value stored
                               in new matrix
else                           % if value of filtered data less than 0.015 the condition ends
end
end                            % end of for loop
I = find (d~=0);               % finds non-zero values
d=d(I);                        % rewrites the matrix with non-zero values
clc
plot (d)
g=mean (d)                     % finds mean
```

REFERENCES

[1] E. L. F. W. Koehler IV, L. H. Kidder, and E. N. Lewis, "Near infrared spectroscopy: the practical chemical imaging solution," *Spectroscopy Europe,* vol. 14/3, 2002.

[2] A. V. B. H. R. Eggert, "Optical properties of human brain tissue, meninges, and brain tumors in the spectral range of 200 to 900nm," *Neurosurgery,* vol. 21, pp. 459-464, 1987.

[3] P. Gurnani, "Near infrared spectroscopic measurement of human and animal brain structures," Masters of Science, Biomedical Engineering, University of Texas Arlington, 2003.

[4] P. C. S. A. N. Yaroslavsky, I. V. Yaroslavsky, R. Schober, F. Ulrich, and H-J Schwarzmaier "Optical properties of selected native and coagulated human brain tissues in vitro in the visible and near infrared spectral range " *Phys. Med. Biol.,* vol. 47, pp. 2059-2073, 2002.

[5] O. M. A. Roggan, C. Schroder, G. Muller, "Determination of optical tissue properties with double integrating sphere technique and Monte Carlo simulations," *Proc. SPIE,* vol. 2100, 1994.

[6] C. A. G. M Johns, D. C. German, and H. Liu, "Determination of reduced scattering coefficient of biological tissue from a needle-like probe," *Optics Express,* vol. 13, pp. 4828-4842, 2005.

[7] A. D. K. R. W. Berg, "Vibrissa movement elicited by rhythmic electrical microstimulation to motor cortex in the aroused rat mimics exploratory whisking," *J. Neurophysiol.,* vol. 90, pp. 2950-2963, 2003.

[8] A. Abdo, M. Sahin, "NIR light penetration in unfrozen samples of rat brain gray matter," *Bioengineering, Proceedings of the Northeast Conference,* vol. art. no. 4967665, 2009.

[9] H. Radhakrishnan, "Use of near infrared and visible spectroscopies to determine optical properties of rat nervous system," Master of Science, Biomedical engineering, University of Texas Arlington, 2006.

[10] M. J. C. Giller, and H. Liu, "Use of intracranial near-infrared probe for localization during stereotactic surgery for movement disorders," *Neurosurgery,* vol. 110, pp. 263-273, 2009.

[11] S. A. P. W-F Cheong, and A. J. Welch, "A review of the optical properties of biological tissues," *IEEE Journal of Quantum Electronics,* vol. 26, pp. 2166-2185, 1990.

[12] T. D. J. S. Dam, P. E. Fabricius, and S. Andersson-Engels, "Multiple polynomial regression method for determination of biomedical optical properties from integrating sphere measurements," *Applied Optics,* vol. 39, pp. 1202-1209, 2000.

[13] J. D. B. J. D. Enderle, and S. M. Blanchard, *Introduction to biomedical engineering*, 2nd ed., 2005.

[14] J. C. J. Amit D Mehta, Benjamin A Flusberg and Mark J Schnitzer, "Fiber optic in vivo imaging in the mammalian nervous system," *Current Opinion in Neurobiology,* vol. 14, pp. 617–628, 2004.

[15] S. Zahedi, "Analytical Comparison of Various Fiber-Optic CDMA Receiver Structures," *JOURNAL OF LIGHTWAVE TECHNOLOGY,* vol. 18, pp. 1718-1727, 2000.

[16] "http://www.pacificcable.com/Fiber-Optic-Tutorial.html," Accessed on May-05-2012.

[17] C. K. Y. Leung, "Fiber optic sensors in concrete: the future?," *NDT&E International,* vol. 34, pp. 85-94, 2001.

[18] "http://www.belden.com/techdatas/metric/M9B037.pdf," Accessed on May-02-2012.

[19] "http://www.bockoptronics.ca/industrial/pdfs/stockeryale/dls_dlsc.pdf," Accessed on March-21-2012.

[20] A. Ersen, "Temperature elevations due to NIR exposure in the brain tissue " Master of Science, Biomedical Engineering, New Jersey Institute of Technology, 2012.

[21] "http://www.rp-photonics.com/gaussian_beams.html," Accessed on April-25-2012.

[22] A. Abdo, "*In vitro* feasibility testing of floating light-activated microelectrical stimulators," Master of Science, Biomedical Engineering, New Jersey Institute of Technology, 2007.

[23] R. Sahu, "Matlab user interface for neural stimulation and recording applications with a laser control.," Master of Science, Biomedical Engineering, New Jersey Institute of Technology, 2011.

[24] "http://sine.ni.com/psp/app/doc/p/id/psp-68/lang/en," Accessed on 02 May, 2012.

[25] A. Abdo and M. Sahin, "Feasibility of Neural Stimulation With Floating-Light-Activated Microelectrical Stimulators," *Biomedical Circuits and Systems, IEEE Transactions on,* vol. 5, pp. 179-188, 2011.

[26] D. S. A. Roggan, U. Netz, J-p. Ritz, C.-T. Germer, and G. Muller, "The effect of preparation technique on the optical parameters of biological tissue," *Appl. Phys.,* vol. 69, pp. 445-453, 1999.

[27] W. C. L. S. C. Gebhart, and A Mahadevan-Jansen, "*In vitro* determination of normal and neoplastic human brain tissue optical properties using inverse adding-doubling," *Phys. Med. Biol.,* vol. 51, pp. 2011-2027, 2006.

[28] L. S. R. Ellingsen, "Optical properties of human brain," *Photochemistry and Photobiology* vol. 38, pp. 293-299, 1983.

[29] A. Abdo, M. Sahin, "Feasibility of neural stimulation with floating-light-activated microelectrical stimulators," *IEEE Transactions on Biomedical Circuits and Systems,* vol. 5, 2011.

[30] H. Sharma, Hoopes, P., "Hyperthermia induced pathophysiology of the central nervous system," *Int. J. Hyperthermia,* vol. 19, pp. 325-354, 2003.